Numerical Simulations of Atherosclerotic Plaque Growth Using Experimental Data

Carolina Brites Ramos[1], Jorge Filipe Duarte Tiago[2], Ana Rosa Miranda dos Santos Silva Herdade[3]

[1]Instituto Superior Técnico, Lisboa, Portugal, carolina.ramos@tecnico.ulisboa.pt
[2]Instituto Superior Técnico, Lisboa, Portugal, jftiago@math.tecnico.ulisboa.pt
[3]Instituto de Bioquímica Molecular, Lisboa, Portugal, anarmsilva@medicina.ulisboa.pt

Abstract

Atherosclerosis is a cardiovascular disease characterized by the formation and progression of a lipid plaque inside the arterial wall innermost layer (intima). Originated by a long chronic inflammation, the lesion involves different biological agents according to stages of plaque development. For a better understanding of this pathology, the present study combines mathematical, experimental and computational approaches. Aiming at visualizing plaque growth, a novel mathematical approach is suggested, starting from previous studies to describe, through partial differential equations, cells and species which intervene in atherosclerosis. Our focus regards the way the continuous accumulation of massive cells (macrophages, foam cells and smooth muscle cells) and collagen fibres are modeled inside the intima. To describe a first phase-approach for future arterial stenosis monitorization in atherosclerotic mice, an experimental procedure was performed on healthy mice models. Intravital microscopy was used to record luminal monocytes endothelial adherence and posterior transmigration (crucial events in atherogenesis). Moreover, to evaluate intima volume growth, we resorted to an idealized rectangular geometry. The complex geometry of left main coronary artery bifurcation is also provided to study blood dynamics, specially focusing on wall shear stress role. Finally, an extensive research of model parameters origin and a sensitivity analysis to access their influence on the obtained results is also provided. Results show robust consistency with literature; however, the use of accurate human physiological parameters still remains a challenge.

Keywords: Atherosclerotic plaque, mathematical modelling, advection-reaction-diffusion equations, sensitivity analysis, intravital microscopy.

1. Introduction

Cardiovascular Diseases (CVDs) are the leading cause of morbidity and mortality worldwide [1], [2]. Asymptomatic at the beginning, atherosclerosis is a type of CVD, commonly referred as a chronic inflammatory disease once it involves an auto-amplification phenomenon. It leads to the formation and progression of a lipid plaque inside vessels intima [3].

The atheroma plaque grows into the arterial lumen, creating a lumen-occluding thrombus (the so-called blood clot) which might block luminal flow, thus, compromising oxygen supply to tissues (ischemic areas) [4], [5]. Also, it can travel to other parts of the circulatory system, triggering cardiovascular events such as embolism (lung), myocardial infarction (heart) or stroke (brain). Moreover, chronic pathologies like coronary heart disease, carotid artery disease, peripheral artery disease or chronic kidney disease might be observed [3], [6], [5]. Researchers believe that atherosclerosis starting point is endothelial dysfunction, triggered by high plasma levels of cholesterol and glycose (or hyperglycemia), hypertension, obesity, infectious and smoking agents [7], [8]. Complex pathological processes are encompassed through different cells and species, namely endothelial cells (ECs), mono chemoattractant protein 1 (MCP-1), monocytes, macrophages, foam cells, oxidized LDL (oxLDL), smooth muscle cells (SMCs) and collagen fibres. Atherosclerosis can be divided in accordance with plaque development stages and experiments have suggested a division of four stages [9]. Accordingly, initial Endothelial Dysfunction (Stage I) is triggered by local hemodynamic alterations (lower wall shear stress[1] values), increasing intima permeability to luminal LDL and monocytes, which accumulate inside the arterial wall, giving rise to the inflammatory reaction [8]. The unprotected oxidative environment starts oxidizing LDL

[1]Force per unit area exerted by blood on the endothelial surface of arterial walls.

(oxLDL) which enhances cytokines expression by ECs. MCP-1, for instance, binds to luminal monocytes, regulating their motion to lesion sites (chemotaxis) [10], [11]. Posteriorly, monocytes transmigrate into the intima (diapedesis) and start differentiating into macrophages [6]. Oxidized LDL particles are recognized and engulfed by macrophages, creating the so-called foam cells[2] [3].

Foam cells start accumulating inside the intima, producing additional cytokines and giving rise to a Fatty Streak (Stage II). Foam cells enhance the persistent inflammation, leading to new monocytes recruitment [7], [3], [6]. The chronic inflammation also triggers circulating platelets adhesion which leads ECs to segregate platelets derived growth factor (PDGF). Consequently, the endothelium fails to inhibit SMCs from proliferating and migrating from the media into the intima, a chemotactic motion regulated by MCP-1 and PDGF [12], [13]. Hence, atherosclerotic lesion evolves into a Fibrofatty Injury (Stage III). Advanced plaque grows and starts invading the lumen, changing vessel geometry and creating the so-called stenosis [11].

SMCs synthetize collagen which also contributes for plaque growth. As one of the main components of extracellular matrix (ECM), collagen exerts the vital mechanical strength inside the plaque, assuring cap's integrity [5]. The lesion develops, thus, into a Fibrous and Mature Plaque (Stage IV) and, eventually, apoptotic cells (ECs, macrophages, foam cells and SMCs) end up releasing their content (necrotic core), which accelerates or induces plaque disruption [13].

2. Methodology

Following previous authors procedures, we present a complete work regarding complex systems of partial differential equations (PDEs), computations and experiments, mainly focused on atheroma plaque growth. After searching for model parameters origin, a sensitivity analysis technique is also provided to access parameters influence on the obtained results.

2.1. Experimental Approach

The lack of clinical data is a common concern among researchers. Some model parameters are hardly measured *in-vivo*, resulting in the computation of crudely estimated values [14], [15], [16]. We performed an experimental procedure with one healthy mouse which can be a first phase-approach for further work on accessing model parameters using the ideal atherosclerotic mice model (apolipoprotein E deficient or ApoE$^{-/-}$, as reported in [17]).

2.1.1. Animals

One Lys-EGFP-ki[3] mouse with 18 weeks old was used in this work [18]. The mouse was kept in an animal facility with a 12 h light/dark cycle and housed in cages in a temperature-controlled room. It was kept on a diet standard mouse food and water ad libitum. The animal received human care in accordance with the Directive of the European Community 2010/63/EU, that mentions the protection of animals used for economic and other scientific ends, also according to the Portuguese Legislation Law 113/2013.

2.1.2. Intravital Imaging

For the surgical procedures and microcirculatory measurements, the healthy mouse was anesthetized intraperitoneally (i.p.) with a cocktail of xylazine/ketamine ($0.1\ mL/10\ g$ of BW). Body temperature was maintained between 35 and 37 °C with auto-regulated heating platform. The surgical procedures for intravital microscopy were made in an appropriate support as described and used by Silva et al in [19]. In our experiments, the abdominal aorta was exposed by opening the peritoneal cavity and gently pushing organs to the side. After this surgical preparation the support with the animal was placed in a multi-photon confocal microscope Leica SP8 MP (Leica, Germany) adapted for intravital microscopy, equipped with a 20×water objective and a 10×ocular. The exposed tissue was superfused with Krebs–Henseleit buffer with $NaHCO_3$ at 37°C bubbled with 95% N_2 and 5% CO_2 and the excess of liquid was removed with a vacuum system. All the images were recorded using the LAX software for offline analysis.

Different parts of the aorta were recorded to verify the presence or not of areas with atherosclerotic plaques. From the recorded images the interactions between leukocytes and endothelial cells were also quantified by the parameters already established: number of rolling leukocytes and their rolling speed, number of adherent leukocytes and vessel diameter [20]. The leukocytes were assumed to be rolling on the endothelium if they were moving at a slower speed than the erythrocytes in the same vessel over 1 min duration. A leukocyte was considered adherent to the endothelium if it remained stationary for more than $30\ s$ in a $100\ \mu m$ length [19].

2.1.3. Blood Quantification

After performing this experimental procedure, a sample of $100\ \mu L$ of abdominal arterial blood was removed to undergo a spectrophotometry method for

[2]These cells have a *foamy* appearance owing to their cytoplasm saturated with a lipid content.

[3]EGFP indicates enhanced green fluorescent protein.

the quantification of blood LDL levels. At the end of the experiment, the animal was euthanized with a pentobarbital injection $100\ mg/kg$ of BW.

2.2. Mathematical Approach

After a cautious review of literature, we decided to extend the work developed by Silva et al. in [21], which lacks advanced plaque modeling. For that, we gathered strong assumptions previously reported by authors on this field but, simultaneously, we suggested some changes to guarantee consistency with assumptions.

2.2.2. Governing Equations Inside the Intima Layer

Our mathematical approach inside the intima layer is detailed according to stages of plaque development.

Endothelial Dysfunction (Stage I)

Following up the work proposed by Silva et al. in [21], Stage I main players are oxLDL, macrophages and MCP-1. Intima oxLDL concentration (L_{ox}) can be described by the reaction-diffusion (R-D) equation:

$$\underbrace{\frac{\partial L_{ox}}{\partial t}}_{} + \underbrace{\nabla \cdot \left(-d_{L_{ox}} \nabla L_{ox}\right)}_{\text{Diffusion}} = \underbrace{-\, k_{ox,M} \frac{L_{ox}}{L_{ox}+K_{L_{ox}}} M}_{\text{Ingestion by macrophages}} \quad (1)$$

where $d_{L_{ox}}$ represents oxLDL diffusion coefficient and $k_{ox,M}$ accounts for oxLDL ingestion rate by macrophages. Degradation term is linear in macrophages (M) and saturating in oxLDL (as concluded in [22]) once $K_{L_{ox}}$ stands for the limit of oxLDL ingestion rate by 1 macrophage. Macrophages evolution (M) can be modeled by a chemotaxis-advection-reaction-diffusion (χ-C-R-D) equation:

$$\underbrace{\frac{\partial M}{\partial t} + \nabla \cdot (\boldsymbol{v} M)}_{\text{Advection}} + \underbrace{\nabla \cdot \left(-d_M \nabla M + \chi_M M \nabla M_{cp}\right)}_{\substack{\text{Diffusion and Chemotactic} \\ \text{motion in response} \\ \text{to MCP-1 signal}}} = \underbrace{M_{pro} M}_{\text{Proliferation}} - \underbrace{k_F \frac{L_{ox}}{L_{ox}+K_{L_{ox}}} M}_{\substack{\text{Degradation due} \\ \text{to foam cells}}} \quad (2)$$

where we assume that macrophages contribute for the inflammatory process, as expected from our assumptions. d_M stands for macrophages diffusion coefficient, M_{pro} for proliferation (natural movement within an inflamed environment) rate and χ_M for their chemotaxis sensitivity parameter in response to MCP-1 gradient (∇M_{cp}). Additionally, macrophages degradation arises from foam cells formation (at rate k_{F_c}) and it is linear in M and saturating in L_{ox}.

Once oxLDL reaches a given threshold, inflammatory signal (starred by MCP-1) is produced. Its intima concentration (M_{cp}) is given by the R-D equation:

$$\underbrace{\frac{\partial M_{cp}}{\partial t} + \nabla \cdot \left(-d_{M_{cp}} \nabla M_{cp}\right)}_{\text{Diffusion}} = \underbrace{k_{M_{cp},M} M}_{\substack{\text{Synthesis by} \\ \text{macrophages}}} + \underbrace{k_{M_{cp},F_c} F_c}_{\substack{\text{Synthesis by} \\ \text{foam cells}}} - \underbrace{\lambda_{M_{cp}} M_{cp}}_{\text{Degradation}} \quad (3)$$

where we assume MCP-1 production by macrophages and foam cells (F_c), so $k_{M_{cp},M}$ and k_{M_{cp},F_c} are their respective rates. $d_{M_{cp}}$ stands for MCP-1 diffusion coefficient and $\lambda_{M_{cp}}$ for its degradation rate.

Fatty Streak (Stage II)

After ingesting large amounts of oxLDL, macrophages transform into lipid laden cells, or foam cells (F_c). Their intima concentration evolution follows the work proposed by Hao and Friedman in [16], with the convection-reaction-diffusion (C-R-D) equation:

$$\underbrace{\frac{\partial F_c}{\partial t} + \nabla \cdot (\boldsymbol{v} F_c)}_{\text{Advection}} + \underbrace{\nabla \cdot \left(-d_F \nabla F_c\right)}_{\text{Diffusion}} = \underbrace{k_F \frac{L_{ox}}{L_{ox}+K_{L_{ox}}} M}_{\text{Formation}} - \underbrace{\lambda_F F_c}_{\text{Degradation}} \quad (4)$$

where d_F stands for foam cells diffusion coefficient, λ_F for degradation rate and, again, contribution for intima volume is considered (advection term). In the formation term, $K_{L_{ox}}$ evidences that F_c are controlled by the upper limit to oxLDL ingestion by one macrophage. The rate of oxLDL uptake by macrophages is, though, different from the rate of foam cells creation because the consumption of oxLDL does not transform macrophages immediately into foam cells.

Fibrofatty Injury (Stage III)

Atherosclerotic advanced plaques in Stage III were already modeled in many works such as [16]. Following those authors, the evolution of SMCs concentration (S) is described by the following χ-C-R-D equation:

$$\underbrace{\frac{\partial S}{\partial t} + \nabla \cdot (\boldsymbol{v} S)}_{\text{Advection}} + \underbrace{\nabla \cdot \left(-d_S \nabla S\right)}_{\text{Diffusion}} = \underbrace{-\nabla \cdot \left(S \chi_C \nabla M_{cp}\right)}_{\substack{\text{Chemotactic} \\ \text{motion by} \\ \text{MCP-1}}} \underbrace{- \nabla \cdot \left(S \chi_C \nabla G\right)}_{\substack{\text{Chemotactic} \\ \text{motion by} \\ \text{PDGF}}} \quad (5)$$

where the advection term is considered owing to SMCs relevant mass for intima volume growth. Furthermore, d_S stands for SMCs diffusion coefficient and χ_C accounts for chemotactic parameter. Chemotactic motion in response to MCP-1 and PDGF gradients (∇M_{cp} and ∇G) is, thus, represented. The same authors modeled intima PDGF dynamics. This cytokine (G) can be described by the R-D equation:

$$\underbrace{\frac{\partial G}{\partial t} + \nabla \cdot \left(-d_G \nabla G\right)}_{\text{Diffusion}} = \underbrace{k_{G,M} M}_{\substack{\text{Production by} \\ \text{macrophages}}} + \underbrace{k_{G,F} F_c}_{\substack{\text{Production} \\ \text{by foam} \\ \text{cells}}} + \underbrace{k_{G,S} S}_{\substack{\text{Production} \\ \text{by SMCs}}} - \underbrace{\lambda_G G}_{\text{Degradation}} \quad (6)$$

where PDGF production rates $k_{G,M}$, $k_{G,F}$, and $k_{G,S}$ refer to macrophages, foam cells and SMCs (respectively). d_G stands for PDGF intima diffusion coefficient and λ_G represents its degradation rate.

Fibrous and Mature Plaque (Stage IV)

Stage IV is remarkably distinguished by collagen fibres synthesis, the key variable for plaque maturation and cap's integrity. For collagen description, we resorted to the model suggested by Cilla et al. in [14], which addresses collagen intima concentration evolution (C_{ol}) through the C-R equation:

$$\underbrace{\frac{\partial C_{ol}}{\partial t} + \nabla \cdot (\boldsymbol{v} C_{ol})}_{\text{Advection}} = \underbrace{k_{C_{ol}} S}_{\text{Production by SMCs}} \tag{7}$$

where $k_{C_{ol}}$ is the collagen synthesis rate by (migrated) SMCs and, again, the advection term is considered.

Plaque Growth

Providing the continuous intima creation and accumulation of cells and species, medium pressure and plaque growth in the y-direction are crucial factors in advanced plaques. This leads us to the main novelty of this work: An improved Stokes system. As far as we know, previous authors have restricted the modeling of plaque growth to foam cells creation and accumulation [23], [15], [21]. Instead, we assume that massive cells such as foam cells, macrophages, collagen and smooth muscle cells contribute for the inflammation. Hence, these players PDEs include an advection term, where $\boldsymbol{v}$ corresponds to the plaque growth velocity. Let us consider a constant A, which stands for the number of cells (per unit volume) inside the intima, such that:

$$A = M(x,y,t) + F_c(x,y,t) + S(x,y,t) + C_{ol}(x,y,t) + Z(x,y,t) \tag{8}$$

where all variables have already been introduced except for Z (biomass) which can be described by:

$$\frac{\partial Z}{\partial t} + \nabla \cdot (vZ) = 0 \tag{9}$$

A general concentration (C_i) verifies:

$$\frac{\partial C_i}{\partial t} + \nabla \cdot (vC_i) - \nabla \cdot (d_i \nabla C_i) = R_i(C_i) \tag{10}$$

where the advection term includes velocity $\boldsymbol{v}$ (passive cellular transport inside the intima). Diffusion terms depend on each diffusion coefficient and reaction terms include production, degradation and chemotaxis.

Assuming that A is constant in time and space one obtains:

$$\frac{\partial A}{\partial t} = 0 \tag{11}$$

which, considering (8) and (10), yields:

$$\nabla \cdot v = \frac{1}{A} \sum_{i=1}^{5} \nabla \cdot (d_i \nabla C_i) + R_i(C_i) \tag{12}$$

To determine $\boldsymbol{v}$ (the model unknown), the system is closed by defining a kind of Stokes Equation, such as the one proposed by Calvez et al. in [15]:

$$\begin{cases} -\nabla \cdot D(v) + \nabla p = 0, & x \in \Omega_i, \ t \in [0,T] \\ \nabla \cdot v = \frac{1}{A} \sum_{i=1}^{5} \nabla \cdot (d_i \nabla C_i) + R_i(C_i), & x \in \Omega_i, \ t \in [0,T] \\ D(v) n_i - p n_i = 0, & x \text{ on } \Gamma_{end}, \ t \in [0,T] \\ v = 0, & x \text{ on } \partial\Omega_i \backslash \Gamma_{end}, \ t \in [0,T] \end{cases} \tag{13}$$

where p represents the intima pressure (which is also a model unknown) and $\boldsymbol{D}$ (the rate of deformation tensor or strain rate tensor) stands for the symmetric part of velocity gradient and it is defined as:

$$\boldsymbol{D}(\boldsymbol{v}) = \frac{1}{2}[\nabla \boldsymbol{v} + (\nabla \boldsymbol{v})^T] \tag{14}$$

The intima is approximated to a continuum medium by linear momentum and mass balance equations, under a local matter incompressibility assumption[4].

2.2.3. Governing Equations Inside the Lumen

Blood Flow Dynamics

Blood is a very complex fluid with peculiar mechanical properties [24]. However, following the blood simplification considered by many authors, we neglect the shear deformation applied to arterial walls and assume blood as a Newtonian (constant viscosity), laminar, isothermal and incompressible fluid [25], [15], [14]. Although our interest of study is atheromatous plaque formation, there is a time "gap" between lumen and intima dynamics: lesion needs decades to grow whereas time scale of blood regards seconds. Thus, pulsatile characteristic of blood flow might be neglected and steady-state condition is assumed for blood flow (no luminal turbulence nor time variation).

The simple description of blood motion inside the lumen is given by stationary incompressible Navier-Stokes (NS) equations:

$$\begin{cases} (\boldsymbol{u}_l \cdot \nabla)\boldsymbol{u}_l - \nu_l \Delta \boldsymbol{u}_l + \nabla p_l = 0 \\ \nabla \cdot \boldsymbol{u}_l = 0 \end{cases} \tag{15}$$

where the unknowns are $\boldsymbol{u}_l$ (blood velocity field) and p_l (blood pressure). Kinematic viscosity is written as $\nu_l = \frac{\mu_l}{\rho_l}$, where ρ_l stands for blood density. The former equation guarantees the conservation of linear momentum (forces acting on the fluid are in equilibrium) whereas the latter represents the conservation of mass for an incompressible fluid.

Wall Shear Stress

In atherosclerosis, hemodynamic shear stresses distribution is highly nonuniform and plays a significant role [21]. When coupling lumen and intima dynamics, it is relevant to estimate Wall Shear Stress (WSS) real value in a specific arterial region, which can be derived from NS solutions. Providing the preservation of *in vivo*

[4]Local matter incompressibility assumption states that when species are created the intima volume is locally increasing.

vascular ECs is influenced by surface stress generated by blood flow, there is an ordinary approach to compute it [21]. By decomposing the surface stress into normal and tangential components, one obtains the normal stress and the apical frictional force (the so-called shear stress, deforming cells in flow direction), respectively. Therefore, WSS can be defined as the tangential component of normal fluid stress at the endothelium: (16)

$$\boldsymbol{WSS} = \boldsymbol{T}_l^n - (\boldsymbol{T}_l^n \cdot \boldsymbol{n}_l)\boldsymbol{n}_l$$

where $\boldsymbol{T}_l^n = \boldsymbol{T}_l \cdot \boldsymbol{n}_l$.

2.2.4. Boundary Conditions

Inside lumen domain (see Figure 2), homogeneous Dirichlet boundary condition (BC) is assumed at the arterial wall (Γ_{end}), that is, zero blood velocity is assumed ($u = 0$). At the luminal inlet ($\Gamma_{l,in}$), entering velocities are given by Poiseuille velocity profile:

$$\boldsymbol{U} = \left(u_{max}\left(1 - \left(\frac{y - r_l}{r_l}\right)^2\right), 0\right) \quad (17)$$

Inside the intima, at Γ_{end} variables are assigned homogeneous[5] Neumann (flux) boundary conditions, with some exceptions (non-homogeneous Neumann BC) based on previous authors assumptions [25], [16], [21] and [14]. In Stage I, oxLDL intima concentration is subject to:

$$\left(-d_{L_{ox}}\nabla L_{ox}\right) \cdot \boldsymbol{n}_i = P_{LDL}\, r_{ox}\, C_{LDL} \quad (18)$$

where a high LDL influx (C_{LDL}) is taken as the starting point for oxLDL oxidation and an oxidation rate (r_{ox}) is assumed. Endothelial permeability (EP) to circulating LDL (P_{LDL}) and monocytes (P_m) are defined as:

$$P_{LDL/m}(WSS, M_{cp}) = P_{LDL/m}^{st} + \frac{\epsilon_{LDL/m}^{max}}{2}\left(\frac{WSS_0}{WSS_0 + WSS} + \frac{M_{cp}}{K_{M_{cp}} + M_{cp}}\right) \quad (19)$$

where $K_{M_{cp}}$ refers to MCP-1 natural saturation rate, WSS_0 stands for standard value of WSS and, finally, $\epsilon_{LDL/m}^{max}$ is given by the difference between the maximum EP and its standard value ($P_{LDL/m}^{max} - P_{LDL/m}^{st}$). WSS stands for WSS magnitude.

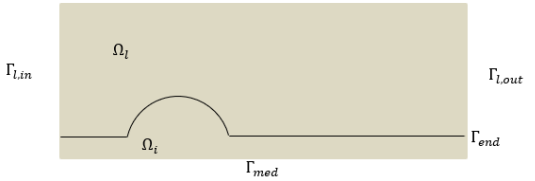

Figure 1 - Illustration of our simple computational domain, where Ω_l represents the lumen, Ω_i the intima, $\Gamma_{l,in}$ and $\Gamma_{l,out}$ the inlet and outlet luminal boundaries (respectively) and, finally, Γ_{end} and Γ_{med} stand for the endothelial and media boundaries (respectively).

Besides, regarding macrophages dynamics, its BC includes P_m and r_{diff} (monocytes differentiation rate into macrophages). Similarly, a given monocytes endothelial influx (C_m) is considered: (20)

$$\left(-d_M\nabla \mathrm{M} + \chi_M M\nabla M_{cp} + \nu M\right) \cdot n_i = P_m\, r_{diff}\, C_m$$

Our model assumes that EP affects intima concentration of oxLDL and macrophages. Hence, we followed Silva and coauthors in [21], defining EP as decreasing function of WSS and increasing function of MCP-1. Furthermore, MCP-1 is also subject to BC at Γ_{end}, defining the endothelial activation once oxLDL concentration is greater than a given threshold (L_{ox}^{th}):

$$\left(-d_{M_{cp}}\nabla M_{cp}\right) \cdot \boldsymbol{n}_i = a_{M_{cp},L_{ox}}(L_{ox} - L_{ox}^{th}) \quad (21)$$

where $a_{M_{cp},L_{ox}}$ stands for MCP-1 segregation rate by ECs. the inflammatory process activation only occurs when oxLDL concentration (L_{ox}) is greater than L_{ox}^{th}. At Γ_{med}, non-homogeneous Neumann (flux) BC was also considered in Stage III for SMCs dynamics:

$$\left(-d_S\nabla S + \boldsymbol{\nu} S\right) \cdot \boldsymbol{n}_i = \alpha_S\,(S_0 - S) \quad (22)$$

where $\alpha_S = \tilde{\alpha}_S \frac{M_{cp}+G}{P_0+G_0}$, with $\tilde{\alpha}_S$ standing for the media influx rate of SMCs into the intima. P_0 and G_0 refer to media MCP-1 and PDGF concentrations (respectively), and SMCs constant media influx is represented by S_0.

Furthermore, both $\Gamma_{l,in}$ and $\Gamma_{l,out}$ were assigned Neumann (flux) boundary conditions, homogeneous for all variables. Finally, in Stokes system all species are assumed to have zero velocity on every boundary except for the endothelial barrier, which deforms into the arterial lumen with velocity ν, allowing plaque growth into the arterial lumen.

2.3. Parameters Selection

To access model parameters, extensive research was conducted throughout experimental studies (available in literature) on atherosclerosis. However, some adaptations were performed to allow biologically reasonable results. Table 2 lists parameters physiological meaning, origin (experimental, estimated or adapted), reference of the work where they were obtained and used values for numerical simulations.

2.4. Computational Approach

To perform numerical simulations and access our model accuracy on modeling atherosclerotic plaque growth, we resorted to COMSOL Multiphysics version 5.0, a commercial finite element solver and simulation software for the solution of PDEs (see [26] for more details). In a first simplified approach, we implemented the model in an idealized 2D rectangular geometry of a coronary artery, representing the intima longitudinal section (see Figure 2). Then, specific features were considered according to clinical studies in [27] and [28]

[5]Homogeneous Neumann (flux) boundary conditions mean that no flux is imposed, that is, $(-d_i\nabla C_i) \cdot \boldsymbol{n}_i = 0$.

regarding physiological dimensions of human coronary artery (left anterior descending or LAD). Then, in a second approach, we resorted to a more complex geometry (left coronary artery bifurcation) where blood dynamics was studied, specially WSS patterns.

For spatial discretization of PDEs, we resorted to the finite element method (FEM), a strong tool to approximate solutions of numerical model equations to the real solution to PDEs. FEM discretization is based on their variational (or weak) formulation, which requires lower continuity on the solution. Applying it to our system and taking $R(C)$ as the reaction/chemotactic term of a generic concentration C, d as its diffusion coefficient and h as its non-homogeneous Neumann (flux) boundary condition, the system yielded:

$$\int_\Omega d\,\nabla C\cdot\nabla\psi\,dx-\int_\Omega R(C)\,\psi\,dx-\int_{\partial\Omega_N} h\,\psi\,dS=0 \quad (23)$$

for a generic A-R-D equation with a non-homogeneous Neumann boundary condition. Representing intima growth velocity vector by $\boldsymbol{u}$ and intima pressure by p, Stokes system was written as:

$$\begin{cases}\int_\Omega \mathbf{D}(\boldsymbol{u}):\nabla\psi\,dx-\int_\Omega p\,\nabla\psi\,dx=0\\ \int_\Omega(\nabla\cdot\boldsymbol{u})\,\psi\,dx-\int_\Omega\frac{1}{A}\sum_{i=1}^{4}\nabla\cdot(d_i\nabla C_i)+R_i(C_i)\;\psi\,dx=0\end{cases} \quad (24)$$

where the four massive protagonists are assumed to contribute for the inflammation. Finally, considering that $\boldsymbol{u}_l$ represents blood velocity, p_l blood pressure and ν_l kinematic viscosity, NS equations were given by:

$$\begin{cases}\int_\Omega(\boldsymbol{u}_l\cdot\nabla)\boldsymbol{u}_l\,\psi\,dx-\int_\Omega \nu_l\mathbf{D}(\boldsymbol{u}_l):\nabla\psi\,dx+\int_\Omega p_l\,\nabla\psi\,dx=0\\ \int_\Omega(\nabla\cdot\boldsymbol{u}_l)\,\psi\,dx=0\end{cases} \quad (25)$$

Backward differentiation formulas (BDF) of order 2 were used for temporal discretization. Once the original geometry grows due to mass addition, *Deformed Geometry* interface was useful to allow domain volume change. Finally, we resorted to Arbitrary Lagrangian-Eulerian (ALE) formulation to couple the deformation with NS equations.

3. Results and Discussion

3.1. Experimental Results

We measured the body weight (BW) of the Lys-EGFP-ki mouse to calculate the administered dose of i.p. anesthesia. Once the obtained value for the BW was, approximately, $26.30 \pm 2.3\,g$, it determines an anesthesia dose of about $270\,\mu L$.

Resorting to LAX software and after recorded frames analysis, we obtained *in vivo* images of mouse leukocytes movement within the abdominal aorta. The Lys-EGFP-ki mouse strain that was used in this work has fluorescent neutrophils due to the presence of a GFP protein in the lysozyme gene. Figure 2 provides a sequence of the intravital microscopy images obtained from the abdominal aorta. In those images we identify the presence of rolling and some adherent neutrophils. The dashed white lines were drawn to facilitate the identification of arterial walls, where no atherosclerotic plaques or accumulation of neutrophils is observed.

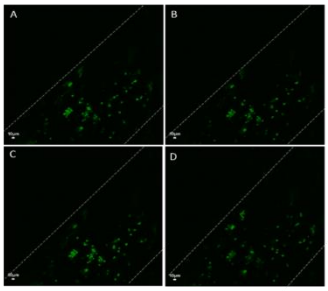

Figure 3 - Abdominal aorta intravital microscopy sequence of images (A – D). White dashed lines indicate the arterial walls and green dots correspond to rolling and some adherent neutrophils.

At the end of the trial, we removed blood from the mouse abdominal aorta to determine LDL circulating levels through a spectrophotometry method and the obtained value was $1.0\ mmol/L$.

By overcoming logistic and financial difficulties, future work should perform this surgical procedure using ApoE$^{-/-}$ mice models, so that model parameters are closer to their real values in mice atherosclerotic plaques (which can be the starting point for extrapolation for human physiological conditions). From the obtained images, we believe that, by using a more adequate mice model with the suitable age and diet, we could visualize neutrophils endothelial adherence, transmigration and posterior accumulation inside the intima layer.

3.2. Numerical Results

Finite dimensional subspace was accomplished through discretization of the intima model into 39 900 triangular elements. The luminal domain, in turn, was discretized into 20 271 triangular elements.

3.2.1. Intima Concentration of Species

Zero initial conditions were considered for all intima variables. To estimate lumen domain coupling, WSS magnitude (needed to compute EP) was taken as 50% of its normal value, according to [29]. To visualize plaque growth, total simulation time was five years ($157\,680\,000\,s$). At the penetration region, a very high endothelial influx of LDLs ($1.9\,g/cm^3$) was chosen to speed up the inflammation. The rapid oxidation and diffusion of intima oxLDL (Figure 4(a)) reach a given threshold, leading to ECs activation with inflammatory signal expression (starred by MCP-1), as shown in Figure 4(b). Near the penetration region, MCP-1 increased EP to circulating LDL and monocytes, which

start accumulating inside the intima. In fact, increasing MCP-1 levels triggered luminal monocytes recruitment, posteriorly differentiating into macrophages inside the intima (see Figure 4(c)). Moreover, we also considered macrophages intima proliferation and chemotactic motion (by MCP-1 gradient), displayed in Figure 4(d).

Once macrophages ingest oxLDL, foam cells are continuously created (Figure 5(a)) near the penetration region. Cytokines production is intensified: PDGF is synthetized by macrophages and foam cells (see Figure 6(a)) and, again, new monocytes are recruited due to MCP-1 increase, as expected by literature [21], [14]. Moreover, in Figures 5(b-d), for little more than 5 simulation years during Stage II, it is visible that the continuous accumulation of massive cells near the EC surface (macrophages and foam cells) results in plaque growth which starts deforming the EC surface.

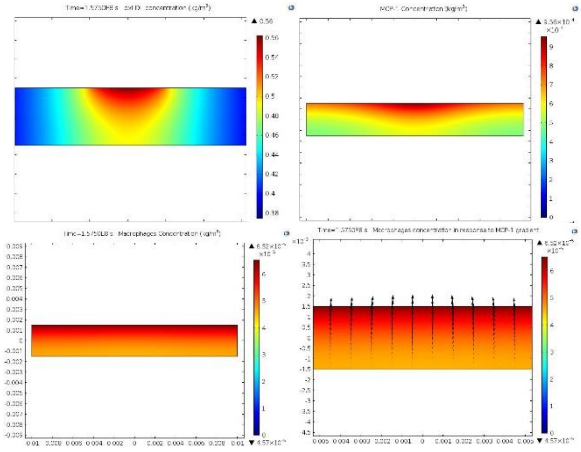

Figure 4 – Intima concentration at $t = 157\,680\,000\ s$ of oxLDL (a), MCP-1 (b) and macrophages (c). Macrophages chemotactic motion in response to MCP-1 gradient (the arrows) is shown in (d).

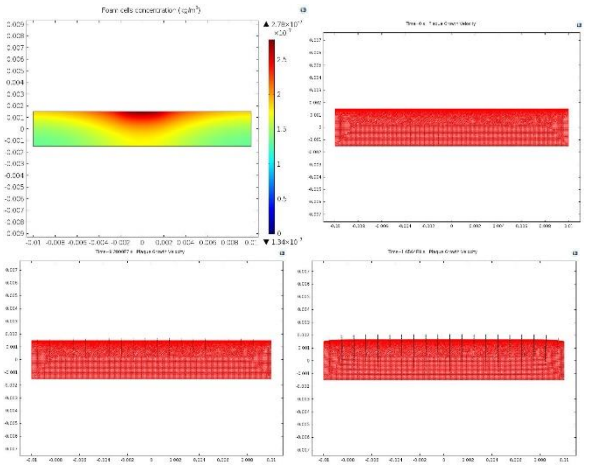

Figure 5 - Intima concentration at $t = 157\,680\,000\ s$ of foam cells (a). Evolution of atherosclerotic plaque growth velocity (the arrows) for times $t = 0\ s$ (b), $t = 82\,800\,000\ s$ (c) and $t = 165\,640\,000\ s$ (d).

Initially, we considered PDGF synthesis by SMCs, but this factor was taken as neglectable during simulations (in good agreement with [1]). Providing the inflammatory signals rapid diffusion, media boundary is, eventually, reached by PDGF and MCP-1. SMCs activation is, consequently, triggered (Figure 6(b)) and ECs fail to prevent SMCs migration. Chemotactic effects in response to those gradients was verified in Figures 6(b-d) and collagen production in Figure 7(a).

In Stages III and IV, for higher times than $t = 170\,020\,000\ s$, we faced a not overcame numerical instability (see the singularity present in Figures 7(b)-(c)). Adapted parameters as well as initial modified conditions to accelerate the inflammation might be important factors for the instability. Besides, once chemotactic motion towards EC surface (expected from [30]) is moderately visible, the obtained results are inconclusive regarding this topic. Therefore, coupling Stage III with the ALE deformation was not performed,

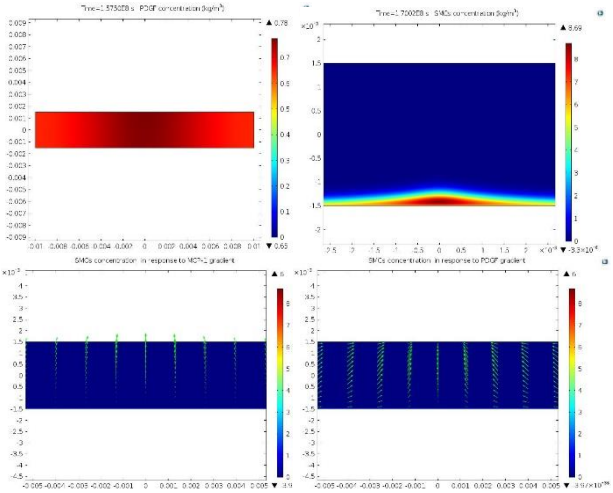

Figure 6 - Intima concentration at $t = 157\,680\,000\ s$ of PDGF (a) and at $t = 170\,020\,000\ s$ of SMCs (b). SMCs motion in response to MCP-1 (c) and PDGF (d) gradients (the arrows) are represented for $t = 79\,000\,000\ s$.

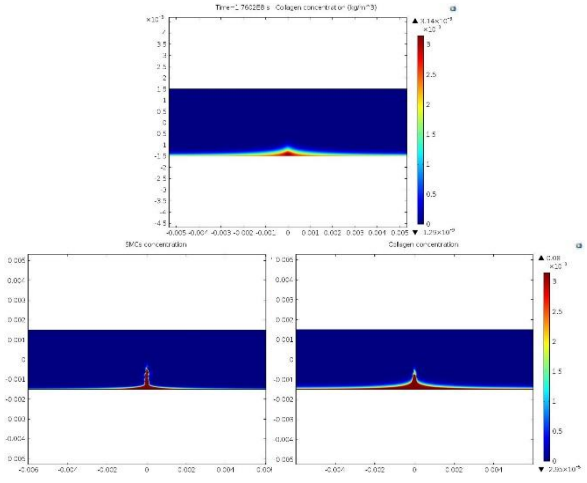

Figure 7 – Intima concentration of collagen at $t = 176\,020\,000\ s$ (a). For $t = 189\,320\,000\ s$, SMCs (b) and collagen (c) singularity is shown.

thus, it should be the subject of future work.

3.2.2. Blood dynamics in LM coronary artery bifurcation

Left anterior descending (LAD) artery is considered a high-risk lesion with restenosis approaching nearly 50% after percutaneous coronary intervention (PCI)

[31]. Thus, to study blood behavior, left main (LM) coronary artery bifurcation was computed, dividing into LAD and left circumflex (LCx) arteries. Dimensions and angles correspond to human physiology reported in [32]. According to literature, lower WSS values define atheroprone regions in arteries (probable endothelial areas for LDL and monocytes entrance) [29]. We assume that EP is decreasing function of WSS. Therefore, to access its behavior, WSS pattern was computed along the red endothelial region highlighted in Figure 8 (a). A zoom view of the obtained results is shown in Figure 8 (b).

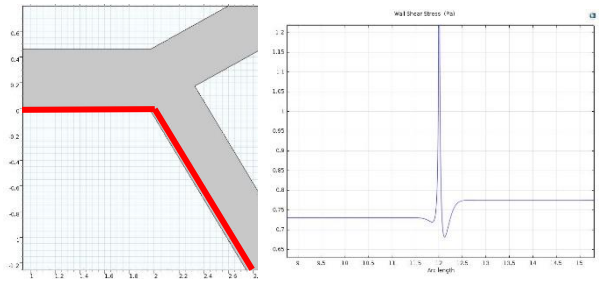

Figure 8 - Endothelial region (highlighted in red) where WSS magnitude was computed (a) and zoom view of WSS magnitude along blood separation region (b).

Hemodynamic shear stresses distribution is spatially nonuniform, which is in accordance with literature. However, it is not entirely described as expected. In fact, as reported by Silva et al. in [14], after bifurcation region, WSS magnitude should return to its standard value (along LM artery). Still, this complex geometry is accurate enough for future coupling with intima subdomain, allowing WSS magnitude computation. After this coupling, WSS influence on the EP pattern can be accessed. Finally, solutions of NS equations are provided below: luminal blood velocity (with streamlines) and blood pressure.

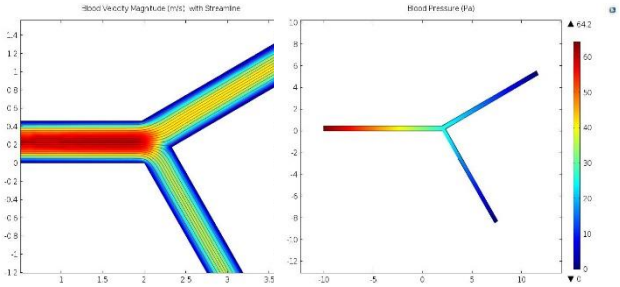

Figure 9 – Blood velocity magnitude (a) and pressure (b) inside LM coronary artery bifurcation with its streamlines profile.

3.3. Sensitivity Analysis

To critically analyze the obtained results, we accessed the robustness of our model providing parameters uncertainty. Stationary studies using *Forward Sensitivity* allowed to access parameters influence on model unknowns. Table 1 summarizes the results, by assigning parameters origin (experimental, estimated or adapted) to one category of normalized[6] average sensitivity values: low (<50%) or high (≥50%).

Table 1–Distribution of each parameter origin (experimental, estimated or adapted) between two categories of normalized average sensitivity values: high (≥50%) and low (<50%).

Average Sensitivity Value	Experimental	Estimated	Adapted
Low	30,05%	5,56%	11,11%
High	44,44%	5,56%	2,78%

A significant set of experimental parameters were assigned high normalized average sensitivity values (44,44% of the parameters), assuring model robustness. However, high sensitivities were also obtained for estimated and adapted values (in total, 8,34%), arousing for future experimental procedures focusing on parameters determination.

4. Main Conclusions and Future Work

Our model describes atheroma plaque growth for 5 years considering the accumulation of macrophages and foam cells, so it can be considered a step forward towards atherosclerosis study. It is, though, incomplete since we disregarded some atherosclerosis players (such as LDL and monocytes) and processes (like fluid-structure interaction) [33]. Future work should consider other massive cells for plaque growth (like T-cells) [16]. Moreover, Stage III (specially SMCs chemotaxis and haptotaxis effects) should remain the focus on further work as well as higher simulations time once advanced plaques need decades to grow [14].

The utilization of accurate model parameters and posterior validation with clinical data remain urgent challenges. As previously reported in [17], future work could perform the ideal procedure to access experimental parameters needs apolipoprotein E deficient (ApoE$^{-/-}$) mice, allowing to measure monocytes endothelial adherence and transmigration, LDL serum levels, arterial luminal radius, percentage of stenosis, among others. Finally, sensitivity analysis technique should be improved to access the parameters which affect the solution the most (and should be the focus of future experimental procedures).

[6] If p is a parameter and C a model unknown which depends on p, the performed normalization of sensitivity values was accomplished by multiplying the latter ones by p/C, along the entire spatial domain. This is a linear estimation of the percentage change in the output variable C [59]. This normalization is useful for consistent comparison among parameters with different units and magnitudes. Note that a sensitivity of 50% indicates that an increase of 1% on the parameter value will increase the respective model unknown in 50%.

Table 2 - Summary of the parameters used in the model. In the "Experimental" column, "A" stands for animal model and "H" for human model.

Parameter Notation	Physiological Meaning	Value (Units)	Reference	Experimental (A or H)	Estimated
Blood Parameters					
WSS_0	Standard WSS in human coronary artery	*1.1 (Pa)*	[34]	Yes (A)	--
U_{mean}	Mean artery inlet velocity	*24.0 (cm/s)*	[35]	Yes (A)	--
μ_l	Blood viscosity	*$3.5x10^{-2}$ ($gcm^{-1}s^{-1}$)*	[36]	Yes (H)	--
ρ_l	Blood density	*1.05 (g/cm^3)*	[36]	Yes (H)	--
Diffusion Coefficients					
$d_{L_{ox}}$	oxLDL diffusion coefficient	*$8.0x10^{-9}$ (cm^2/s)*	[37]	Yes (H)	--
d_M	Macrophages diffusion coefficient	*$1.0x10^{-11}$ (cm^2/s)*	[38]	Yes (H)	--
$d_{M_{cp}}$	MCP-1 diffusion coefficient	*$2.0x10^{-6}$ (cm^2/s)*	[39]	Yes (H)	--
d_{F_c}	Foam cells diffusion coefficient	*$1.0x10^{-11}$ (cm^2/s)*	[40]	Yes (H)	--
d_S	SMCs diffusion coefficient	*$1.0x10^{-11}$ (cm^2/s)*	[40]	Yes (H)	--
d_G	PDGF diffusion coefficient	*$1.0x10^{-6}$ (cm^2/s)*	[41]	Yes (H)	--
Rates					
$k_{M_{cp},M}$	MCP-1 production rate by macrophages	*$1.0x10^{-10}$ (s^{-1})*	[42]	Yes (H)	--
k_{M_{cp},F_c}	MCP-1 production rate by foam cells	*$3.0x10^{-10}$ (s^{-1})*	[42]	Yes (H)	--
$k_{G,M}$	PDGF production rate by macrophages	*$1.16x10^{-6}$ (s^{-1})*	[43]	Yes (H)	--
k_{G,F_c}	PDGF production rate by foam cells	*$3.82x10^{-7}$ (s^{-1})*	[43]	Yes (H)	--
$k_{G,S}$	PDGF production rate by SMCs	*$5.79x10^{-6}$ (s^{-1})*	[43]	Yes (H)	--
k_{F_c}	Foam cells formation rate	*$1.39x10^{-6}$ (s^{-1})*	[44]	Yes (A)	--
k_{col}	Collagen synthesis rate by SMCs	*$2.16x10^{-11}$ ($gcell^{-1}s^{-1}$)*	[45]	Yes (H)	--
$\lambda_{M_{cp}}$	MCP-1 degradation rate	*$2.31x10^{-5}$ (s^{-1})*	[46]	Yes (H)	--
λ_{F_c}	Foam cells degradation rate	*$3.47x10^{-7}$ (s^{-1})*	[47]	Yes (A)	--
λ_G	PDGF degradation rate	*$4.44x10^{-5}$ (s^{-1})*	[41]	Yes (H)	--
r_{diff}	Monocytes differentiation rate into macrophages	*$1.15x10^{-6}$ (s^{-1})*	[47]	Yes (A)	--
r_{ox}	LDL oxidation rate	*$3.0x10^{-4}$ (s^{-1})*	[48]	Yes (H)	--
M_{pro}	Macrophages proliferation rate	*$1.0x10^{-9}$ (s^{-1})*	[11]	Adapted	Yes
$k_{L_{ox}}$	Saturation rate of oxLDL uptake by one macrophage	*0.5 (g/cm^3)*	[22]	Yes (A)	--
$k_{M_{cp}}$	Saturation rate of MCP-1 due to ingestion by macrophages	*$2.5x10^{-5}$ (g/cm^3)*	[49]	Yes (H)	--
$k_{L_{ox},M}$	Rate of oxLDL uptake by macrophages	*$1.0x10^{-4}$ (s^{-1})*	[11]	--	Yes
$a_{M_{cp},L_{ox}}$	Rate of MCP-1 activation due to high oxLDL concentration	*$1.0x10^{-10}$ (s^{-1})*	[15]	Adapted	Yes
$\tilde{a}_S$	Influx rate of SMCs into the intima	*0.2 (cm^{-1})*	[16]	--	Yes
Concentrations					
C_{LDL}	LDL endothelial source	*1.9 (g/cm^3)*	[50]	Adapted	--
C_m	Monocytes endothelial source	*$5.0x10^{-5}$ (g/cm^3)*	[49]	Yes (H)	--
L_{ox}^{Lh}	Threshold oxLDL concentration	*$8.0x10^{-6}$ (g/cm^3)*	[51]	Yes (H)	--
A	Plaque average density	*1.22 (g/cm^3)*	[52]	Yes (H)	--
S_0	SMCs influx at the media boundary	*$6.0x10^{-3}$ (g/cm^3)*	[53]	Yes (H)	--
P_0	MCP-1 influx concentration	*$3.0x10^{-10}$ (g/cm^3)*	[54]	Yes (H)	--
G_0	PDGF influx concentration	*$1.5x10^{-8}$ (g/cm^3)*	[55]	Yes (H)	--
Others					
χ_C	SMCs chemotaxis sensitivity parameter	*$1.16x10^{-4}$ ($cm^5g^{-1}s^{-1}$)*	[56]	Adapted	--
χ_M	Macrophages chemotaxis sensitivity parameter	*$8.64x10^{-6}$ ($cm^5g^{-1}s^{-1}$)*	[57]	Adapted	--
P_{LDL}^{st}	Standard endothelial permeability to LDL	*$1.07x10^{-11}$ (cm/s)*	[15]	--	Yes
P_{LDL}^{max}	Maximum endothelial permeability to LDL	*$2.09x10^{-8}$ (cm/s)*	[35]	Yes (H)	--
P_m^{st}	Standard endothelial permeability to monocytes	*$1.07x10^{-12}$ (cm/s)*	[21]	--	Yes
P_m^{max}	Maximum endothelial permeability to monocytes	*$5.0x10^{-6}$ (cm/s)*	[58]	Yes (H)	--

5. References

[1] R. Ross, "Inflammation or Atherogenesis," *N. Engl. J. Med.*, vol. 340, no. 2, pp. 115–126, 1999.

[2] O. W. in Data, "Share of Deaths by Cause," 2016.

[3] G. S. Hoffman, C. M. Weyand, C. A. Langford, and J. Goronzy, Eds., *Inflammatory Disease of Blood Vessels*. Wiley-Blackwell, J., 2012.

[4] K. Barrett, H. Brooks, S. Boitano, and S. Barman, *Ganong's Review of Medical Physiology*. 2010.

[5] M. Simionescu and A. V Sima, "Inflammation and Atherosclerosis," pp. 19–38, 2012.

[6] S. Mitrovska, S. Jovanova, I. Matthiesen, and C. Liebermans, *Atherosclerosis: Understanding pathogenesis and challenge for treatment*. 2009.

[7] P. Cullen, J. Rauterberg, and S. Lorkowski, "The Pathogenesis of Atherosclerosis," vol. 1, pp. 3–70, 2005.

[8] A. M. Malek, S. L. Alper, and S. Izumo, "Hemodynamic shear stress and its role in atherosclerosis.," *JAMA*, vol. 282, no. 21, pp. 2035–42, Dec. 1999.

[9] M. A. K. Bulelzai and J. L. A. Dubbeldam, "Long time evolution of atherosclerotic plaques," *J. Theor. Biol.*, vol. 297, pp. 1–10, 2011.

[10] B. Mompeo, D. Popov, A. Sima, E. Constantinescu, and M. Simionescu, "Diabetes-induced structural changes of venous and arterial endothelium and smooth muscle cells.," *J. Submicrosc. Cytol. Pathol.*, vol. 30, no. 4, pp. 475–84, Oct. 1998.

[11] C. Mckay *et al.*, "Towards a Model of Atherosclerosis."

[12] H. Wolinsky and S. Glagov, "A lamellar unit of aortic medial structure and function in mammals.," *Circ. Res.*, vol. 20, no. 1, pp. 99–111, Jan. 1967.

[13] M.-L. Bochaton-Piallat and M. Bäck, "Novel concepts for the role of smooth muscle cells in vascular disease: towards a new smooth muscle cell classification," *Cardiovasc. Res.*, vol. 114, no. 4, pp. 477–480, Mar. 2018.

[14] M. Cilla, E. Peña, and M. A. Martínez, "Mathematical modelling of atheroma plaque formation and development in coronary arteries," 2013.

[15] V. Calvez, J. G. Houot, N. Meunier, A. Raoult, and G. Rusnakova, "Mathematical and numerical modeling of early atherosclerotic lesions," 2010.

[16] W. Hao and A. Friedman, "The LDL-HDL profile determines the risk of

atherosclerosis: A mathematical model," *PLoS One*, 2014.
[17] S. C. Whitman, "A practical approach to using mice in atherosclerosis research.," *Clin. Biochem. Rev.*, vol. 25, no. 1, pp. 81–93, 2004.
[18] N. Faust, F. Varas, L. M. Kelly, S. Heck, and T. Graf, "Insertion of enhanced green fluorescent protein into the lysozyme gene creates mice with green fluorescent granulocytes and macrophages.," *Blood*, vol. 96, no. 2, pp. 719–726, 2000.
[19] a S. Silva, C. Saldanha, and J. Martins e Silva, "Effects of velnacrine maleate in the leukocyte-endothelial cell interactions in rat cremaster microcirculatory network.," *Clin. Hemorheol. Microcirc.*, vol. 36, no. 3, pp. 235–246, 2007.
[20] P. Kubes and S. M. Kerfoot, "Leukocyte recruitment in the microcirculation: the rolling paradigm revisited.," *News Physiol. Sci.*, vol. 16, no. April, pp. 76–80, Apr. 2001.
[21] T. Andrade Freire da Silva Supervisor, A. da Costa Sequeira dos Ramos Silva, and R. B. Neves Ferreira Santos, "Mathematical Modeling of the Atherosclerosis Physiopathology," 2016.
[22] B. Hokland, a J. Mendez, and J. F. Oram, "Cellular localization and characterization of proteins that bind high density lipoprotein.," *J. Lipid Res.*, vol. 33, no. 9, pp. 1335–42, 1992.
[23] V. Calvez, A. Ebde, N. Meunier, and A. Raoult, "Mathematical and Numerical Modeling of the Atherosclerotic Plaque Formation," *ESAIM Proc.*, vol. 28, pp. 1–12, 2009.
[24] L. Formaggia, A. Quarteroni, and A. Veneziani, Eds., *Cardiovascular Mathematics*. Milano: Springer Milan, 2009.
[25] T. Silva, J. Tiago, and A. Sequeira, "Mathematical Analysis and Numerical Simulations for a Model of Atherosclerosis."
[26] "COMSOL Multiphysics," 2014.
[27] J. T. Dodge, B. G. Brown, E. L. Bolson, and H. T. Dodge, "Lumen diameter of normal human coronary arteries. Influence of age, sex, anatomic variation, and left ventricular hypertrophy or dilation.," *Circulation*, vol. 86, no. 1, pp. 232–246, Jul. 1992.
[28] R. N. MacAlpin, A. S. Abbasi, J. H. Grollman, and L. Eber, "Human Coronary Artery Size During Life," *Radiology*, vol. 108, no. 3, pp. 567–576, Sep. 1973.
[29] M. Molavi Zarandi, R. Mongrain, and O. F. Bertrand, "Determination of Flow Conditions in Coronary Bifurcation Lesions in the Context of the Medina Classification," *Model. Simul. Eng.*, vol. 2012, pp. 1–10, 2012.
[30] O. Kocher *et al.*, "Phenotypic features of smooth muscle cells during the evolution of experimental carotid artery intimal thickening. Biochemical and morphologic studies.," *Lab. Invest.*, vol. 65, no. 4, pp. 459–70, Oct. 1991.
[31] S. Kasturi, S. Bandimida, N. Gajiwala, and A. Thakkar, "Case Report A Challenging Case of Bifurcation Lesion in Left Anterior Descending Artery : Managed Successfully with Everolimus-Eluting Bioresorbable Vascular Scaffold and Kissing Balloon Technique under Optical Coherence Tomography Guidance," no. June, pp. 114–116, 2015.
[32] Y. Cui *et al.*, "Quantification of left coronary bifurcation angles and plaques by coronary computed tomography angiography for prediction of significant coronary stenosis: A preliminary study with dual-source CT," *PLoS One*, vol. 12, no. 3, p. e0174352, 2017.
[33] Y. Yang, W. Jäger, M. Neuss-Radu, and T. Richter, "Mathematical modeling and simulation of the evolution of plaques in blood vessels," *J. Math. Biol.*, 2015.
[34] H. H. Lipowsky, S. Usami, and S. Chien, "In vivo measurements of 'apparent viscosity' and microvessel hematocrit in the mesentery of the cat," *Microvasc. Res.*, vol. 19, no. 3, pp. 297–319, May 1980.
[35] U. Olgac, V. Kurtcuoglu, and D. Poulikakos, "Computational modeling of coupled blood-wall mass transport of LDL: effects of local wall shear stress.," *Am. J. Physiol. Heart Circ. Physiol.*, vol. 294, no. 2, pp. H909-19, Feb. 2008.
[36] W. R. Milnor, "Hemodynamics," *Clin. Cardiol.*, vol. 13, no. 11, p. 821a–821a, Nov. 1989.
[37] M. Prosi, P. Zunino, K. Perktold, and A. Quarteroni, "Mathematical and numerical models for transfer of low-density lipoproteins through the arterial walls: a new methodology for the model set up with applications to the study of disturbed lumenal flow," *J. Biomech.*, vol. 38, no. 4, pp. 903–917, Apr. 2005.
[38] M. Chaplain and A. Matzavinos, "Mathematical modelling of spatio-temporal phenomena in tumour immunology: Tutorials in mathematical biosciences III: cell cycle, proliferation, and cancer.," Springer Berlin Heidelberg, Berlin, Heidelberg, 2006.
[39] M. R. Owen and J. A. Sherratt, "Pattern formation and spatiotemporal irregularity in a model for macrophage-tumour interactions.," *J. Theor. Biol.*, vol. 189, no. 1, pp. 63–80, Nov. 1997.
[40] Y. Kim, S. Roh, S. Lawler, and A. Friedman, "miR451 and AMPK mutual antagonism in glioma cell migration and proliferation: a mathematical model.," *PLoS One*, vol. 6, no. 12, p. e28293, 2011.
[41] C. Xue, A. Friedman, and C. K. Sen, "A mathematical model of ischemic cutaneous wounds.," *Proc. Natl. Acad. Sci. U. S. A.*, vol. 106, no. 39, pp. 16782–7, Sep. 2009.
[42] P. Siogkas *et al.*, "Multiscale - Patient-Specific Artery and Atherogenesis Models," *IEEE Trans. Biomed. Eng.*, vol. 58, no. 12, pp. 3464–3468, Dec. 2011.
[43] T. B. Barrett and E. P. Benditt, "Platelet-derived growth factor gene expression in human atherosclerotic plaques and normal artery wall.," *Proc. Natl. Acad. Sci. U. S. A.*, vol. 85, no. 8, pp. 2810–4, Apr. 1988.
[44] B. Vesosky, D. K. Flaherty, and J. Turner, "Th1 cytokines facilitate CD8-T-cell-mediated early resistance to infection with Mycobacterium tuberculosis in old mice.," *Infect. Immun.*, vol. 74, no. 6, pp. 3314–24, Jun. 2006.
[45] H. Zahedmanesh, H. Van Oosterwyck, and C. Lally, "A multi-scale mechanobiological model of in-stent restenosis: deciphering the role of matrix metalloproteinase and extracellular matrix changes," *Comput. Methods Biomech. Biomed. Engin.*, vol. 17, no. 8, pp. 813–828, Jun. 2014.
[46] W. Zhao, C. A. Oskeritzian, A. L. Pozez, and L. B. Schwartz, "Cytokine Production by Skin-Derived Mast Cells: Endogenous Proteases Are Responsible for Degradation of Cytokines," *J. Immunol.*, vol. 175, no. 4, pp. 2635–2642, Aug. 2005.
[47] A. Friedman, J. Turner, and B. Szomolay, "A model on the influence of age on immunity to infection with Mycobacterium tuberculosis.," *Exp. Gerontol.*, vol. 43, no. 4, pp. 275–85, Apr. 2008.
[48] H. Esterbauer, G. Striegl, H. Puhl, and M. Rotheneder, "Continuous Monitoring of in Vztro Oxidation of Human Low Density Lipoprotein," *Free Radic. Res. Commun.*, vol. 6, no. 1, pp. 67–75, Jan. 1989.
[49] C. Bell, *Clinical Guide to Laboratory Tests.*, 3rd ed., vol. 35, no. 11. 2009.
[50] D. C. Schwenke and T. E. Carew, "Initiation of atherosclerotic lesions in cholesterol-fed rabbits. II. Selective retention of LDL vs. selective increases in LDL permeability in susceptible sites of arteries.," *Arteriosclerosis*, vol. 9, no. 6, pp. 908–18.
[51] C. Chen and D. B. Khismatullin, "Oxidized Low-Density Lipoprotein Contributes to Atherogenesis via Co-activation of Macrophages and Mast Cells," *PLoS One*, vol. 10, no. 3, p. e0123088, Mar. 2015.
[52] D. A. Rahdert, W. L. Sweet, F. O. Tio, C. Janicki, and D. M. Duggan, "Measurement of density and calcium in human atherosclerotic plaque and implications for arterial brachytherapy," *Cardiovasc. Radiat. Med.*, vol. 1, no. 4, pp. 358–367, Oct. 1999.
[53] D. C. Miller, A. Thapa, K. M. Haberstroh, and T. J. Webster, "Endothelial and vascular smooth muscle cell function on poly(lactic-co-glycolic acid) with nano-structured surface features.," *Biomaterials*, vol. 25, no. 1, pp. 53–61, Jan. 2004.
[54] J. Rhodes, J. Sharkey, and P. Andrews, "Serum IL-8 and MCP-1 concentration do not identify patients with enlarging contusions after traumatic brain injury.," *J. Trauma*, vol. 66, no. 6, p. 1591–7; discussion 1598, Jun. 2009.
[55] D. F. Bowen-Pope, T. W. Malpass, D. M. Foster, and R. Ross, "Platelet-derived growth factor in vivo: levels, activity, and rate of clearance.," *Blood*, vol. 64, no. 2, pp. 458–69, Aug. 1984.
[56] Y. Kim and A. Friedman, "Interaction of tumor with its micro-environment: A mathematical model.," *Bull. Math. Biol.*, vol. 72, no. 5, pp. 1029–68, Jul. 2010.
[57] Y. Kim, S. Lawler, M. O. Nowicki, E. A. Chiocca, and A. Friedman, "A mathematical model for pattern formation of glioma cells outside the tumor spheroid core.," *J. Theor. Biol.*, vol. 260, no. 3, pp. 359–71, Oct. 2009.
[58] J. Glod *et al.*, "Monocytes form a vascular barrier and participate in vessel repair after brain injury.," *Blood*, vol. 107, no. 3, pp. 940–6, Feb. 2006.
[59] M. a Atherton, R. Bates, M. Perry, M. Oldfield, and H. Wynn, "Sensitivity analysis modelling for microscale multiphysics robust engineering design," no. October 2014, pp. 1–8, 2008.